ACI STRUCTURAL JOURNAL TECHNICAL PAPER

Title No. 117-S135

Diagonally Reinforced Concrete Coupling Beams with Grade 120 (830) High-Strength Steel Bars

by Shahedreen Ameen, Rémy D. Lequesne, and Andrés Lepage

Four large-scale coupling beams were tested under fully reversed cyclic loads to investigate the effects on behavior of diagonal bar grade (60 or 120 [420 or 830]), beam shear stress (9.5 or 14$\sqrt{f_c'}$, psi [0.79 or 1.17$\sqrt{f_c'}$, MPa]), and longitudinal bar detailing (either terminated near the beam-wall interface or developed into the walls). Coupling beam chord rotation capacity was 7.1% for the beam with Grade 60 (420) bars and between 5.1 and 5.6% for the beams with Grade 120 (830) bars, a difference likely due to having hoops spaced at 3.4d_b and 4d_b for Grade 60 and 120 (420 and 830) bars, where d_b is the diagonal bar diameter. Effective stiffness, energy dissipation, and residual chord rotations were approximately inversely proportional to bar grade. Developing the secondary longitudinal reinforcement reduced rotation demands at beam ends but did not improve deformation capacity. Beam shear stress did not affect beam chord rotation capacity.

Keywords: bar buckling; chord rotation capacity; coupled walls; high-strength reinforcement; reversed cyclic load; shear stress.

INTRODUCTION

Structural (shear) walls are often the preferred choice for the lateral force resisting system in reinforced concrete buildings designed for earthquake resistance. Architectural considerations commonly result in wall openings that can divide a single wall into multiple walls connected by short deep beams referred to as coupling beams. Properly designed coupled wall systems have considerably larger stiffness and strength than individual (uncoupled) walls.

Studies of the behavior of coupling beams subjected to displacement reversals have shown that beams reinforced with diagonally oriented reinforcing bars exhibit large strength and deformation capacity.[1,2] For design of such beams, it is assumed that all imposed shear and moment demands are resisted by the diagonal bars, which are enclosed within closely spaced hoops necessary to resist bar buckling. However, diagonally oriented reinforcement creates construction difficulties due to the challenge of placing numerous large bars at an inclination through densely reinforced wall boundary elements. Several alternative reinforcement layouts have been studied to find simpler ways to construct reinforced concrete coupling beams,[3-8] but each has limitations. Fiber-reinforced concrete has also been used successfully to reduce reinforcing bar congestion,[9,10] but incorporating fiber-reinforced concrete requires specific knowledge and has yet to be widely adopted in practice. Steel and composite steel-concrete coupling beams are also a viable option,[11] but constructability can still be a concern: the long embedment required to ensure full development of the steel section must pass through the longitudinal and transverse reinforcement in the wall boundary zone.

Reinforcement congestion and construction difficulties would be reduced if fewer high-strength bars were used instead of conventional Grade 60 (420) bars. However, the ACI Building Code[12] limits the yield stress of coupling beam reinforcement to 60 ksi (420 MPa) due to paucity of experimental data. To examine this solution, results are reported from tests of coupling beams constructed with Grade 120 (830) high-strength steel bars. The test program included the following variables: nominal yield stress of diagonal reinforcement (Grade 60 [420] or Grade 120 [830]), design shear stress (9.5 or 14$\sqrt{f_c'}$, psi [0.79 or 1.17$\sqrt{f_c'}$, MPa]), and embedment length of secondary (non-diagonal) longitudinal reinforcement (bars were either terminated 2 in. [50 mm] from the wall face or extended a length sufficient to develop a stress of 1.25 times the yield stress of the bar at the wall face). The main motivation for the test program was to simplify construction while maintaining or improving overall performance of coupling beams.

RESEARCH SIGNIFICANCE

Results are reported from the first tests of coupling beams reinforced with high-strength Grade 120 (830) steel, which reduces reinforcement congestion and facilitates ease of construction. The effects of diagonal bar grade on chord rotation capacity, beam stiffness, energy dissipation, and residual chord rotation are quantified. Results are also reported from the first test of a coupling beam with an aspect ratio near two, designed for a nominal shear stress of 14$\sqrt{f_c'}$, psi (1.17$\sqrt{f_c'}$, MPa), 40% larger than the ACI Building Code[12] limit. High shear stresses, made feasible with high-strength reinforcement, negligibly affect chord rotation capacity, a finding also observed in other studies at lower shear stresses.[13]

EXPERIMENTAL PROGRAM

Specimens

Four large-scale coupling beam specimens were tested under reversed cyclic displacements. Each specimen consisted of a coupling beam (rotated 90 degrees from horizontal) framing into top and bottom blocks. Details of the coupling beams are listed in Table 1 and shown in Fig. 1

ACI Structural Journal, V. 117, No. 6, November 2020.

MS No. S-2019-460, doi: 10.14359/51728067, received November 23, 2019, and reviewed under Institute publication policies.

and 2. The specimens had a coupling beam clear span of 34 in. (860 mm), overall depth of 18 in. (460 mm), and width of 10 in. (250 mm), resulting in a clear span-to-depth ratio of 1.9. The coupling beams had either Grade 60 or 120 (420 or 830) steel as diagonal reinforcement and Grade 60 (420) steel for all non-diagonally oriented reinforcement, including hoops and crossties.

The transverse reinforcement layout was nominally identical in all coupling beams, with No. 3 (10 mm) hoops and crossties spaced at 3 in. (75 mm) on center, or 3.4 and 4 times d_b, the diameter of the Grade 60 and 120 (420 and 830) diagonal bars, respectively. This amount of transverse reinforcement satisfied ACI 318-14[12] Section 18.10.7.4d. For restraining bar buckling, the ACI 318-14 limit for hoop spacing is $6d_b$ for Grade 60 (420) bars. Because high-strength bars carry higher stress, they require shorter unbraced lengths.[14] If hoop spacing, s, is the unbraced bar length, the Euler buckling equation indicates that bar stress at buckling is inversely proportional to the square of s/d_b. This implies Grade 120 (830) bars require a hoop spacing of $1/\sqrt{2} \times 6d_b = 4.2d_b$ based on code-level buckling restraint for Grade 60 (420) bars. The specimens had hoop spacings of $3.4d_b$ for Grade 60 (420) diagonal bars and $4d_b$ for Grade 120 (830) diagonal bars, which correspond to 55 and 95% of the limit for Grade 60 and 120 (420 and 830) bars. This made the Grade 120 bars more prone to buckling.

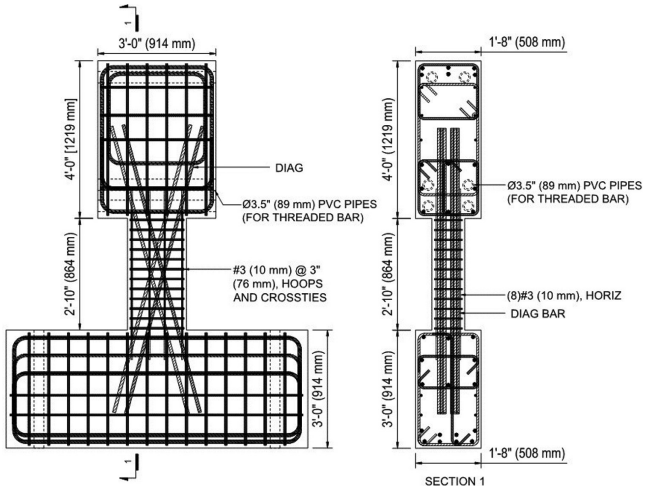

Fig. 1—Specimen details.

Coupling beams CB1, CB2, and CB2D were designed to have nominal shear stresses of approximately $9.5\sqrt{f_c'}$, psi ($0.79\sqrt{f_c'}$, MPa) and CB3D was designed to have a nominal shear stress of $14\sqrt{f_c'}$, psi ($1.17\sqrt{f_c'}$, MPa). Nominal shear stress was calculated with nominal material properties and assuming the diagonal reinforcement resists all imposed shear force. Though design nominal shear stresses were the same for CB1, CB2, and CB2D, CB1 had 12 No. 7 (22 mm) diagonal bars, whereas CB2 and CB2D had eight No. 6 (19 mm) diagonal bars. This 50% reduction in diagonal bar area led to less congestion and easier construction. Furthermore, it would be difficult to construct a coupling beam for shear stresses like in CB3D with Grade 60 (420) reinforcement because the required number of bars would make it very congested.

No. 3 (10 mm) secondary longitudinal bars were distributed around the beam perimeter. To be consistent with the ACI 318-14 Commentary, these secondary bars were terminated 2 in. (50 mm) into the top and bottom blocks of CB1 and CB2. This detail, however, has been shown to result in concentrated rotations (and therefore concentrated bar strains) at the ends of coupling beams.[2,15] In CB2D and CB3D, the No. 3 (10 mm) longitudinal bars were extended a length sufficient to develop a stress of 1.25 times the

Table 1—Summary of coupling beam specimens

Specimen ID	Nominal diagonal bar yield stress, f_y, ksi (MPa)	Design shear stress*, psi (MPa)	Diagonal bars†	Secondary longitudinal bars‡
CB1	60 (420)	9.6 (0.80)	12 No. 7 (22)	8 No. 3 (10 mm) Cutoff§
CB2	120 (830)	9.4 (0.78)	8 No. 6 (19)	8 No. 3 (10 mm) Cutoff§
CB2D	120 (830)	9.4 (0.78)	8 No. 6 (19)	8 No. 3 (10 mm) Developed‖
CB3D	120 (830)	14.0 (1.17)	12 No. 6 (19)	8 No. 3 (10 mm) Developed‖

*Based on ACI 318-14[12] Eq. (18.10.7.4) using nominal material properties (f_y of 60 or 120 ksi [420 or 830 MPa]) and f_c' of 6000 psi (41 MPa).
†Includes all bars from both diagonal bar groups.
‡Grade 60 (420) steel bars.
§Cutoff 2 in. (50 mm) from the beam-wall interface, consistent with ACI 318-14 Commentary.[12]
‖Developed into end blocks per Eq. (25.4.2.3a) in ACI 318-14,[12] using a stress of 1.25 f_y and a confinement term of 2.5.

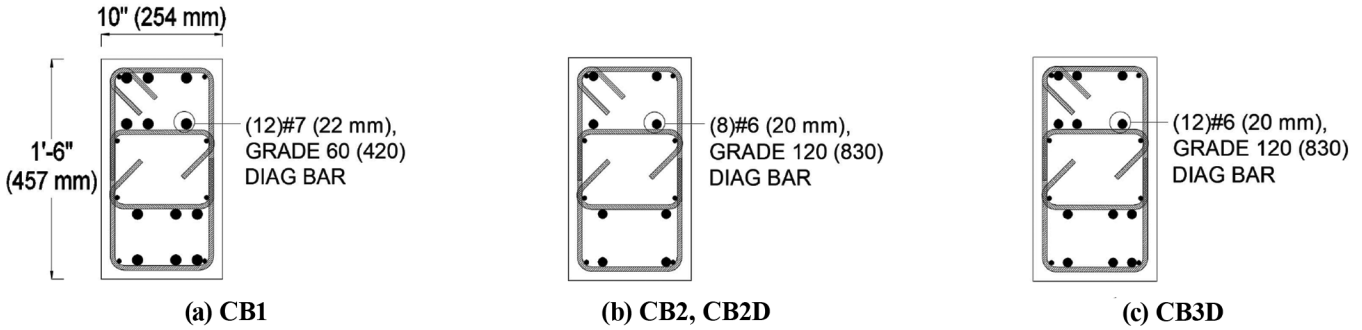

Fig. 2—Coupling beam cross sections near wall intersection. Hoops and crossties are No. 3 (10 mm) Grade 60 (420) bars at 3 in. (75 mm); and secondary longitudinal bars are No. 3 (10 mm) Grade 60 (420) bars.

yield stress of the bar at the beam-wall interface. This was done to better distribute deformations into the beam span, and thereby reduce diagonal reinforcement strain demands. Aiming for reduced strain demands was important because Grade 120 (830) bars have a smaller uniform and fracture elongation than Grade 60 (420) bars.

Materials

Measured concrete and reinforcement properties are given in Table 2. Ready mix concrete from a local supplier was used to monolithically cast the specimens. The concrete had a target compressive strength of 6000 psi (41 MPa) and a maximum aggregate size of 0.75 in. (19 mm). The measured concrete compressive strengths were obtained from tests of standard concrete cylinders following ASTM C39.[16] Concrete mixture proportions are listed in Table 3.

Mill certifications for the Grade 60 (420) and Grade 120 (830) steel bars showed compliance with ASTM A706[20] and ASTM A1035,[21] respectively. Reinforcing bar mechanical properties were obtained from tensile tests in accordance with ASTM A370[17] and ASTM E8.[22] Sample tensile test results are plotted in Fig. 3 as stress versus strain.

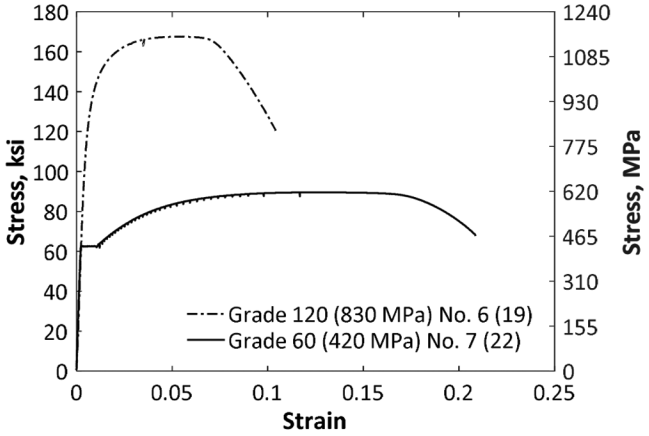

Fig. 3—Measured stress versus strain for diagonal bars.

Test setup and loading protocol

A typical specimen and testing setup are shown in Fig. 4. For testing, the specimen bottom block was bolted to the laboratory strong floor with two 2.5 in. (64 mm) diameter high-strength threaded rods passing through the laboratory strong floor and specimen bottom block. Two hydraulic actuators were used to load the specimens. Each actuator has a stroke length of 40 in. (1020 mm) and a force capacity of 220 kip (980 kN). The actuators were connected to the laboratory strong wall and specimen top block with a series of steel fixtures. Stability of the system was maintained with lateral bracing.

Specimens were subjected to a series of reversed cyclic displacements following the protocol shown in Fig. 5, which was patterned after the protocol recommended in FEMA 461 (2007).[23] To overcome imprecision of relatively small displacement measurements, force-based control was used prior to yielding of the diagonal reinforcement. This consisted of increasing the applied force until the chord rotation was approximately equal to the target values in Fig. 5 and reversing the loading direction. The remainder of the cycles were imposed using displacement control. The ratio between forces or displacements applied by the two actuators was selected such that an inflection point remained near mid-span of the coupling beam throughout the tests (beams were bent in double-curvature). Additional details are provided in Ameen et al.[24]

Instrumentation

An infrared-based non-contact position measurement system was used to record the position in three-dimensional space of 59 optical markers glued to the specimen (Fig. 6). The markers were arranged in a 4 in. (100 mm) square grid pattern over one face of each specimen and part of the top and bottom blocks. Additional markers were used to define coordinates of the laboratory strong floor. The term "layer" refers to the space between two marker rows and the term "station" (the shaded area in Fig. 6) refers to the region surrounded by four adjacent markers. The spatial coordinates of each marker were

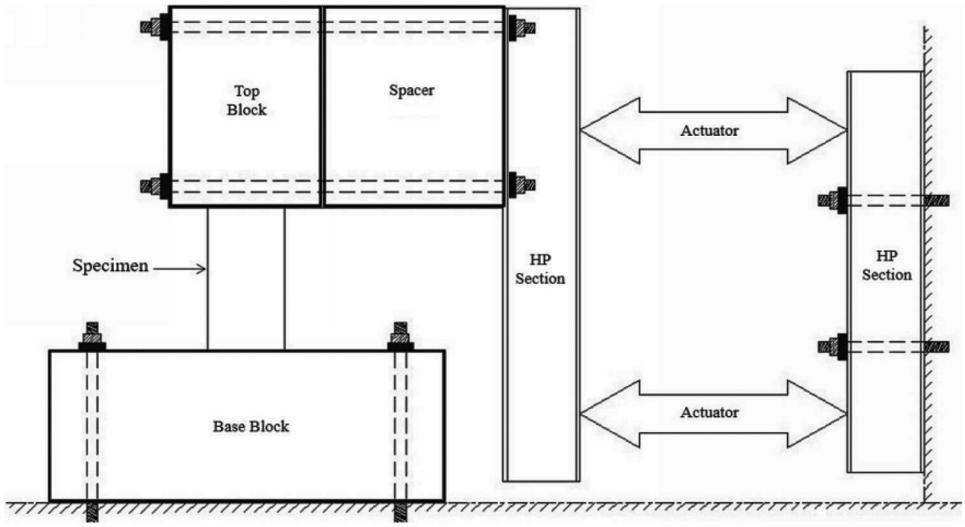

Fig. 4—Schematic of test setup.

triangulated based on infrared light pulses emitted by the markers and detected by cameras. The resulting position data were used to calculate specimen displacements and deformations.

Diagonal, transverse, and longitudinal reinforcing bars were instrumented with 28 electrical resistance strain gauges placed at the locations shown in Fig. 7. In each specimen, two diagonal bars were instrumented with six strain gauges each, 11 strain gauges were attached to the hoops and crossties, and the No. 3 (10 mm) longitudinal bars were instrumented with five strain gauges. The strain gauges were rated for 15% strain to allow measurements throughout the test. Strain gauge data are documented in Ameen et al.[24]

Table 2—Measured material properties and coupling beam capacities

Specimen	Concrete	Diagonal bars		Coupling beam capacities		
ID	Test day compressive strength, f_{cm}*, psi (MPa)	Yield stress, f_{ym}†, ksi (MPa)	Uniform elongation ε_{su}	V_{max}, kip (kN)	$v_{max}/\sqrt{f_c'}$, psi (MPa)	CR_{cap}‡, %
CB1	6000 (41)	63 (434)	12.8%	184 (819)	13.2 (1.10)	7.1
CB2	7200 (50)	128 (883)	5.3%	207 (921)	13.6 (1.13)	5.1
CB2D	6300 (43)	128 (883)	5.3%	204 (907)	14.3 (1.19)	5.3
CB3D	6200 (43)	128 (883)	5.3%	275 (1220)	19.4 (1.61)	5.6

*Mean result from three 4 x 8 in. (100 x 200 mm) cylinders tested following ASTM C39.[16]

†For diagonal bars tested following ASTM A370,[17], based on 0.2%-offset method.

‡Average of CR_{max} attained in each loading direction.

EXPERIMENTAL RESULTS AND DISCUSSION

Specimen response and observations

Measured shear force is plotted versus chord rotation for all coupling beams in Fig. 8. Beam chord rotation was calculated using data from the infrared-based non-contact position measurement system as the relative displacement between top and bottom blocks, corrected for rotation of both the top and bottom blocks, divided by the clear span of the beam. Table 2 lists the maximum shear force, V_{max}; maximum shear stress, v_{max}, divided by the square root of measured concrete compressive strength; and the chord rotation capacity, CR_{cap}, for each specimen. Chord rotation capacity, CR_{cap}, was defined as the average of the maximum chord rotations imposed in each loading direction before the strength diminished to less than 80% of the maximum applied shear (each direction treated separately).

Despite having shear stress demands larger than $13\sqrt{f_c'}$, psi ($1.08\sqrt{f_c'}$, MPa), all four coupling beams exhibited stable behavior until a chord rotation of at least 5%, which exceeds the expected chord rotation capacity based on ASCE 41-17.[25] Control specimen CB1 completed two cycles to 6% chord rotation with minor strength loss. CB1 had a strength loss of more than 20% during the first cycle to 8% chord rotation. The strength loss was due to bar fracture. The deformed shapes of the fractured and adjacent bars were consistent with bar buckling occurring in prior cycles. The test was terminated during the first excursion to 10% chord rotation due to limitations of the testing apparatus. CB2 failed suddenly at 5.2% chord rotation during the first excursion to 6%. This sudden failure was dominated by several fractures of diagonal bars that were preceded by bar buckling, similar to CB1. The larger deformation capacity of CB1 may be attributable to several factors, including: 1) Grade 60 (420) bars carry less stress and are therefore less prone to buckling than Grade 120 (830) bars; 2) CB1, with Grade 60 (420) bars, had a hoop spacing of 3.4 times the diagonal bar diameter, whereas CB2, with Grade 120 (830) bars, had hoops spaced at four times the diagonal bar diameter; and 3) the

Table 3—Batched concrete mixture proportions per cubic yard*

		Cementitious material (*CM*)		Aggregate			Admixtures				
					Coarse						
ID	Water lb	Cement† lb	Fly ash‡ lb	Fine§ lb	A‖ lb	B# lb	Retarder** oz	Water reducer†† oz	Water/*CM*‡‡ lb/lb	Initial slump in.	Spread in.
CB1	284	649	150	1208	507	1177	24	35	0.40	9	18.5
CB2	230	748	0	1727	1111	0	0	30	0.39	6.25	—
CB2D	286	647	150	1196	503	1177	24	35	0.40	11	23
CB3D	286	647	150	1196	503	1177	24	35	0.40	11	23

*Note: $yd^3 = 0.764\ m^3$, 1 lb = 4.45 N, 1 in. = 25.4 mm.

†Type I portland cement.

‡Class C.

§Kansas River sand, meets ASTM C33[18] requirements for fine aggregate.

‖Pea gravel, maximum aggregate size of 3/8 in. (10 mm).

#Crushed limestone, maximum aggregate size of 3/4 in. (19 mm).

**Set retarder (compliant with ASTM C494).[19]

††High-range water-reducing admixture (compliant with ASTM C494).[19]

‡‡Calculated by dividing the weight of water in one cubic yard of concrete, including corrections to account for aggregate moisture content, by total weight of cement and fly ash.

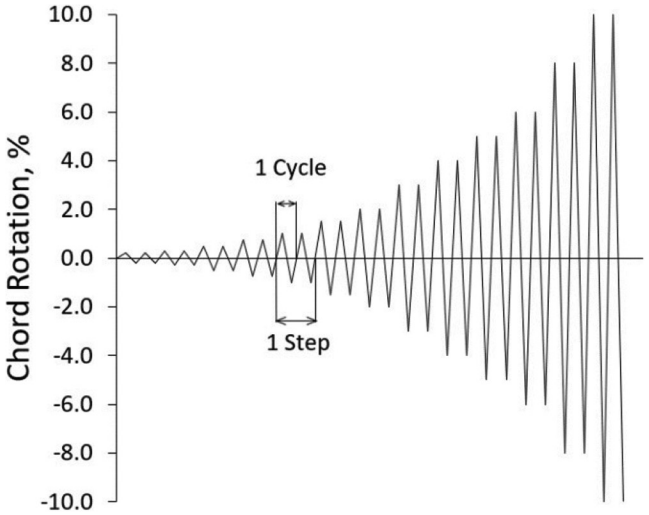

Fig. 5—Loading protocol.

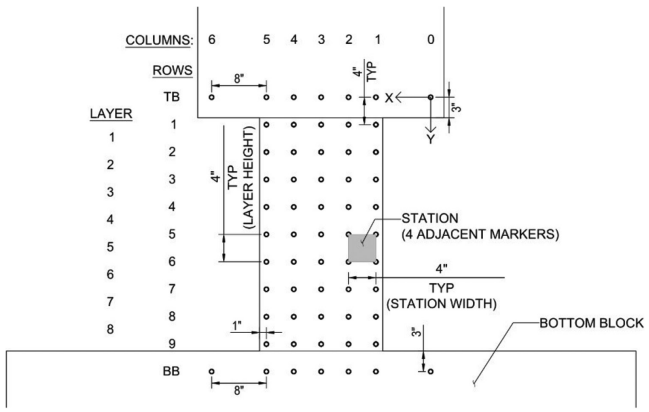

Fig. 6—Locations of optical markers. (Note: 1 in. = 25.4 mm.)

Grade 60 (420) bars in CB1 had larger uniform elongation than the Grade 120 (830) bars in CB2. CB1 also exhibited a larger strength after bar fracture than CB2. This is attributed to CB1 having more diagonal bars, so fracture of one or two bars had a smaller effect on the strength of CB1 than CB2.

CB2D and CB3D, which had the secondary (non-diagonal) longitudinal bars extended into the top and bottom blocks, also exhibited reduced strength at chord rotations larger than 5%. This would suggest that development of the secondary reinforcement for $1.25f_y$ did not have the intended effect of reducing the concentration of rotations near the beam ends, but in fact both CB2D and CB3D exhibited less end rotation and more damage throughout the beam span prior to diagonal bar buckling than either CB1 or CB2. Figure 9 shows CB2 and CB2D after reaching chord rotations near 5%. Damage in CB2 was concentrated at the beam-wall interface where rotations were large and where diagonal bars ultimately fractured. In contrast, CB2D had severe damage near both beam ends, as well as more pronounced cracking and spalling throughout the beam span. Nevertheless, the diagonal bars in CB2D still buckled near the beam ends at a chord rotation similar to CB2. Buckling of diagonal reinforcement therefore controlled the failure of all four coupling beams. It is not clear whether the difference in longitudinal bar detailing (cutoff versus developed) would have improved the chord

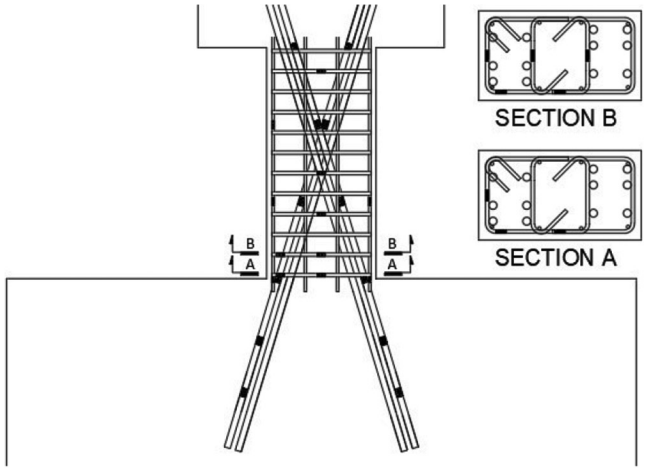

Fig. 7—Strain gauge layout.

rotation capacity had bar buckling been better restrained by means of closer spacing of transverse reinforcement near the beam ends. Given that bar buckling preceded bar fracture in the tests of all four specimens, and bar fracture commonly follows bar buckling regardless of uniform elongation when cyclic loads are imposed, the difference in uniform elongation between Grade 60 (420) and 120 (830) bars appears to have had limited impact on the deformation capacity of the tested beams. Similar observations were reported by others for structural walls.[26]

For the tested beams, the maximum applied shear corresponded to a shear stress significantly larger than the design shear stress. CB1, CB2, and CB2D resisted shear stresses of 13.2, 13.6, and $14.3\sqrt{f_c'}$ psi (1.10, 1.13, and $1.19\sqrt{f_c'}$ MPa) respectively, compared to design shear stresses near $9.5\sqrt{f_c'}$ psi ($0.79\sqrt{f_c'}$ MPa). CB3D resisted a shear stress of $19.4\sqrt{f_c'}$ psi ($1.61\sqrt{f_c'}$ MPa), compared to a design shear stress of $14\sqrt{f_c'}$ psi ($1.17\sqrt{f_c'}$ MPa). These larger-than-expected shear stresses may result in larger-than-expected axial force demands in the adjacent structural walls and therefore may need to be considered in design. Regardless, the deformation capacity of well detailed diagonally reinforced coupling beams was not sensitive to shear stress, as CB2D and CB3D exhibited similar deformation capacities.

Relative contribution of different components of chord rotation

Data from the optical markers attached to the surface of each specimen were analyzed to quantify the specimen deformations attributable to flexural rotation, beam-end rotation, shear, and sliding at the beam ends. Flexural rotation was calculated for each layer throughout the test as the difference between the rotations of the lines defined by the end markers of two consecutive rows. Deformation due to beam-end rotation refers to the relative rotation between the first row of markers on the beam (rows 1 or 9, Fig. 6) and those located on the end blocks (rows TB or BB, Fig. 6). Beam-end rotation includes strain penetration into the end blocks and flexural rotation associated with the 1 in. (25 mm) layer between the face of the end block and the row of markers at the beam ends. Shear deformation of each layer was taken as the average angular distortion calculated

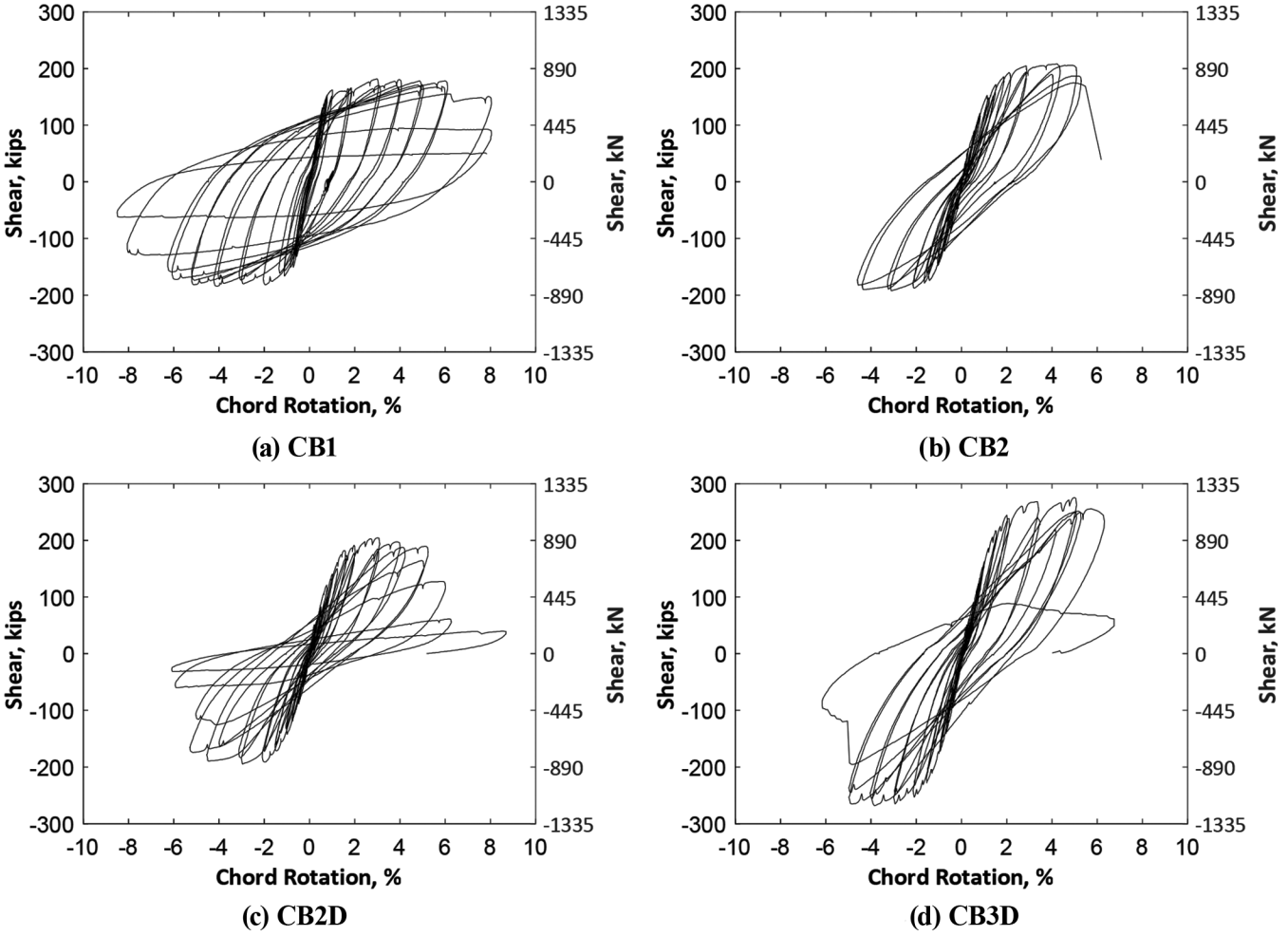

Fig. 8—Shear versus chord rotation.

for each of the four stations in a layer. Sliding was calculated as the difference between horizontal displacements of the row located on an end block and the adjacent row on the coupling beam (rows 1 or 9 in Fig. 6). Details of the calculations are documented in Ameen et al.[24]

Figure 10 shows the calculated contributions to total chord rotations of the four deformation mechanisms considered: flexural rotation, beam-end rotation, shear deformation, and sliding. The contributions are plotted cumulatively, such that their sums approach unity.

Figure 10 shows that the four mechanisms had a similar share of deformations for CB1 and CB2, the specimens with secondary (non-diagonal) longitudinal bars terminated near the beam-wall interface. Beam-end rotation accounted for a large portion (45 to 90%) of the total chord rotation. In general, flexural rotations, shear deformations, and sliding accounted for less than 35, 25, and 15% of the total chord rotations, respectively. The overwhelming importance of beam-end rotation, which includes strain penetration, is consistent with results from prior tests of diagonally reinforced coupling beams with secondary (non-diagonal) longitudinal reinforcement terminated near the wall face.[2]

The longer embedment of the non-diagonal reinforcement in CB2D and CB3D resulted in reduced beam-end rotations and increased flexural rotations and shear deformations

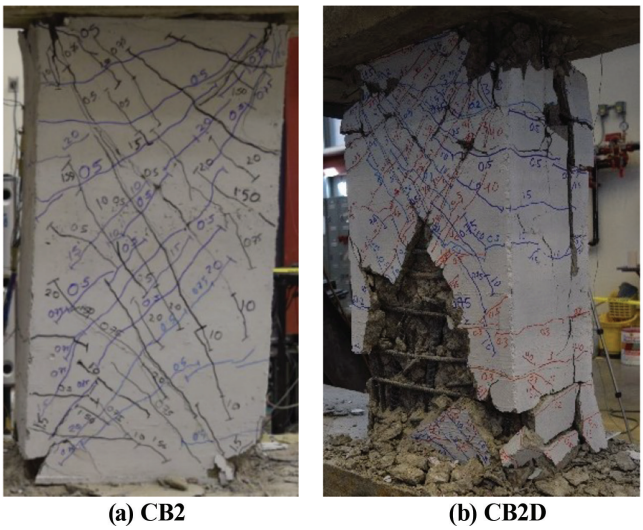

Fig. 9—Coupling beam condition near 5% chord rotation.

compared with CB1 and CB2. This is shown in Fig. 10, where the contributions to total chord rotation of flexure, beam-end rotation, shear, and sliding were generally limited to 35, 50, 50, and 10%, respectively. The difference in deformation contributions is consistent with the difference in damage distributions described previously. However, the change in detailing (cutoff versus developed) did not

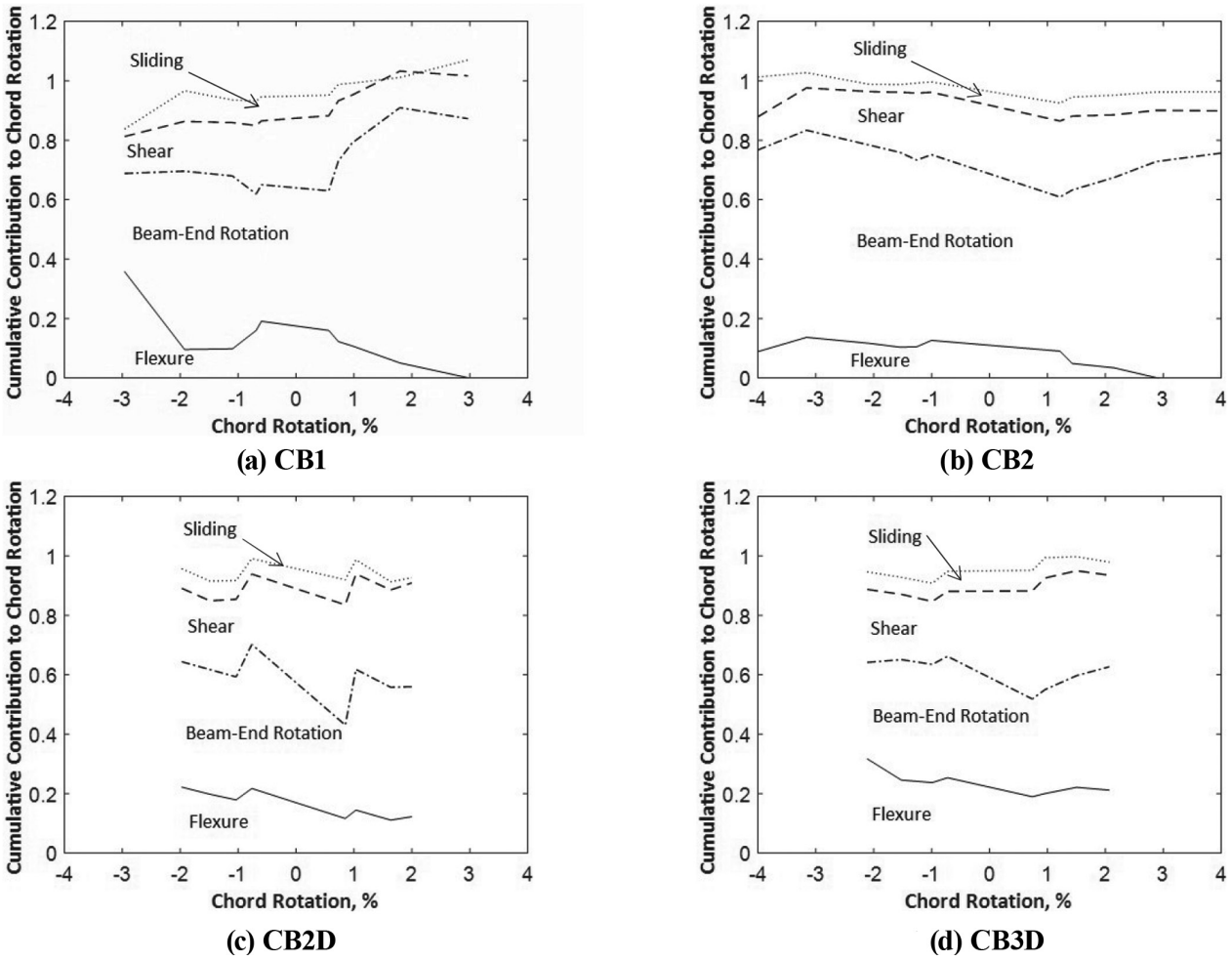

Fig. 10—Cumulative contribution to chord rotation versus chord rotation.

increase chord rotation capacity, which was controlled by bar buckling followed by fracture.

Stiffness

Envelopes of the measured shear force versus chord rotation data for each coupling beam are shown in Fig. 11. The envelopes represent line segments linking the points of peak shear attained during each step of the loading protocol (refer to Fig. 5). Figure 11 shows that the initial (uncracked) stiffnesses of the coupling beams are similar. After cracking, the secant stiffness of CB1 is slightly larger than that of the others, especially at shear forces between 100 and 150 kips (445 and 670 kN). This small but consistent difference in stiffness was correlated with the amount of diagonal reinforcement. Between 100 and 150 kips (445 and 670 kN), the chord rotations were smallest for CB1, larger for CB3D, and largest for CB2 and CB2D, which had similar shear force-chord rotation envelopes up to 5% chord rotation.

The envelopes of the shear versus chord rotation data were used to estimate the effective stiffness of all four coupling beams. Effective stiffness was defined as the slope of a secant drawn from the origin to the intersection of the envelope of shear versus chord rotation and a horizontal line at 75% of the maximum shear for each loading direction. This definition[27] was used because it is simple and because the

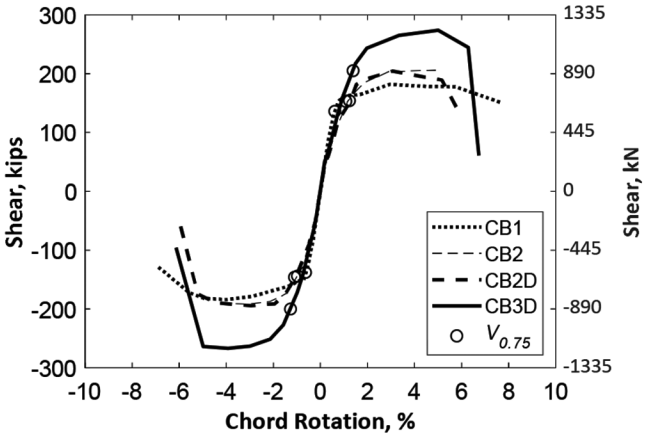

Fig. 11—Envelopes of shear versus chord rotation.

tangent stiffness of the shear versus chord rotation envelopes notably decreased after this point (refer to Fig. 11).

An effective moment of inertia (I_{eff}) was defined as $V_{75}l_n^2/(12E_cCR_{75})$, where V_{75} and CR_{75} are the shear and chord rotation at 75% of the maximum shear force in each loading direction. This approach uses I_{eff} to represent shear, bar slip, and flexural deformations, like the approach used by Elwood and Eberhard[28] for columns. Values of I_{eff}/I_g are shown in Fig. 12 for each coupling beam and loading direction. The ratios were approximately 0.1 for CB1 and 0.06 for CB2, CB2D,

and CB3D. Values of I_{eff} for beams with high-strength Grade 120 (830) reinforcement were therefore approximately three-fifths of I_{eff} for the beam with conventional Grade 60 (420) reinforcement.

Hysteretic energy dissipation

A hysteretic energy dissipation index, E_h, was used to examine how reinforcement grade and detailing (cutoff versus developed) affected the hysteretic energy dissipated by the coupling beams. E_h was calculated as the area W enclosed under the shear versus chord rotation curve during the second cycle of each loading step, divided by $2\pi D_m V_m$, where D_m and V_m are the peak chord rotation and shear imposed in that cycle. E_h represents the equivalent viscous damping factor of a linear-elastic system capable of dissipating energy (W) in one cycle under steady-state oscillation.[29]

Figure 13(a) shows E_h versus chord rotation for all four coupling beams. E_h was larger for CB1 than for the other beams at chord rotations larger than 1%. Between 3 and 5% chord rotation, E_h was approximately twice as large for CB1 as for the other beams. Therefore, E_h was approximately inversely proportional to the yield stress of the diagonal reinforcement. This is further demonstrated in Fig. 13(b), which shows that all four coupling beams had similar E_h for a given value of chord rotation times $60/f_{ym}$ in ksi ($420/f_{ym}$ in MPa). This observation indicates that E_h is a function of plastic deformation, which for a given chord rotation is smaller for a beam having higher grade of reinforcement with higher yield stress.

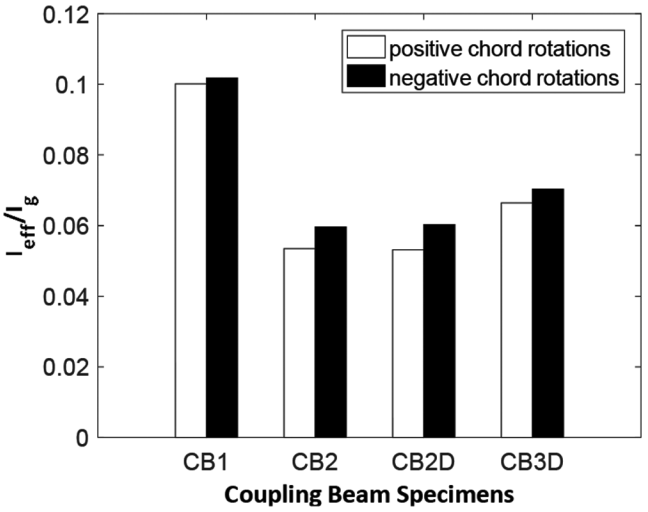

Fig. 12—Effective moment of inertia I_{eff} *normalized by gross moment of inertia* I_g.

Residual chord rotations when unloaded

Buildings with large residual deformations after strong earthquakes often require rehabilitation or demolition. Although the residual deformation of an isolated member is an imperfect measure of residual building drift, coupling beams with smaller residual chord rotations would be less likely to contribute to residual building drift. Residual coupling beam chord rotation is defined as the chord rotation

Table 4—Force-deformation envelopes for nonlinear seismic analysis

Parameters*	Envelope A* ASCE 41-17[25] and ACI 369.1-17[30]	Envelope B* TBI[31]	Recommended envelope*
c	0.8	0.8	0.8
d	0.03	0.03	0.03
e	0.05	0.05	0.05
I_{eff}/I_g	0.3†	0.07 (l_n/h)‡	0.07 (l_n/h) $(60/f_y)$
Q_y	V_n§	V_n§	V_n§
Q_C	V_{pr}‖	V_{pr}‖	V_{pr}‖

*Refer to Notation.
†Based on Table 10-5 of ASCE 41-17.[25]
‡Based on Table 4-3 of TBI.[31]
§Based on ACI 318-14[12] Eq. (18.10.7.4) using expected material properties. Figures 16 and 17 are based on f_{cm} and 1.1 f_y and a diagonal bar inclination of 18 degrees.
‖Based on ACI 318-14[12] Eq. (18.10.7.4) using a diagonal bar stress of 1.25 f_y. Figures 16 and 17 are based on a diagonal bar inclination of 18 degrees.

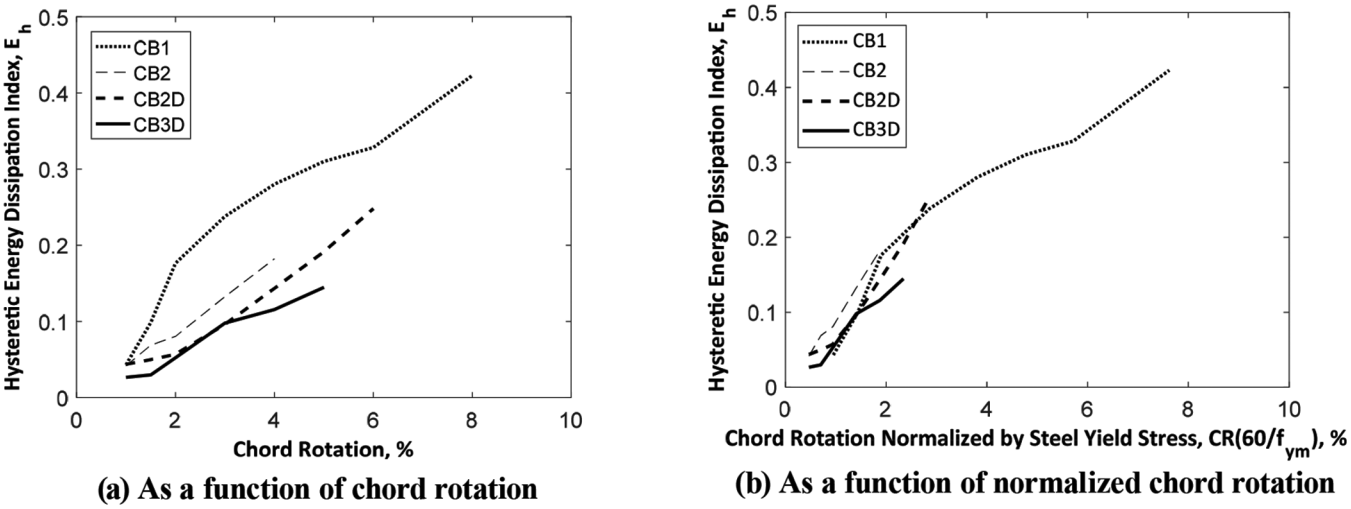

Fig. 13—Hysteretic energy dissipation index.

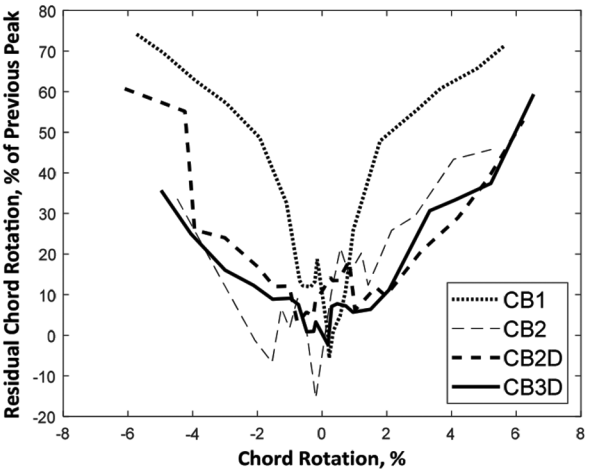

(a) As a function of chord rotation

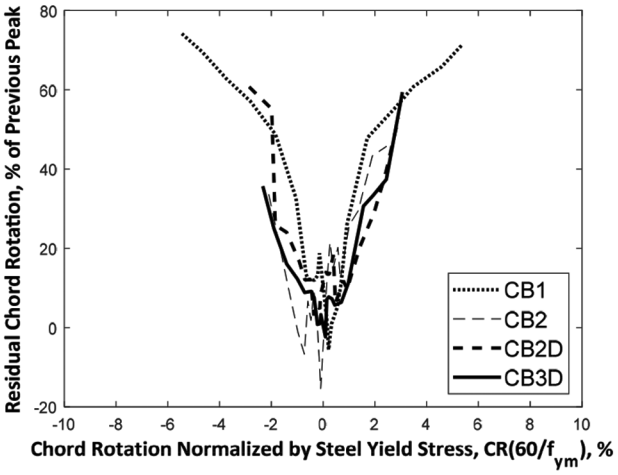

(b) As a function of normalized chord rotation

Fig. 14—Residual chord rotation.

at zero shear force after unloading from a larger chord rotation demand. For comparisons between all four coupling beams, the residual chord rotation after each loading cycle is divided by the largest prior chord rotation within the same loading cycle. Figure 14(a) shows this ratio, calculated for the second cycle of loading to each target drift, plotted versus the peak chord rotation within each half cycle of loading.

Starting from 1% chord rotation, large differences were evident between CB1, with conventional Grade 60 (420) diagonal reinforcement, and the other coupling beams. For instance, near 4% chord rotation, the average residual chord rotations for CB2, CB2D, and CB3D were approximately 30% of the prior peak in both loading directions. For CB1, near the same target chord rotation of 4%, the residual chord rotation was approximately 60% of the prior peak. Furthermore, it appears that residual chord rotations of isolated coupling beams decrease in approximately inverse proportion to reinforcement yield stress. Figure 14(b) shows that residual chord rotations are similar among the specimens for a given value of chord rotation times $60/f_{ym}$ in ksi ($420/f_{ym}$ in MPa).

In summary, while the use of high-strength bars (compared with conventional Grade 60 [420] bars) decreases effective stiffness (Fig. 12) and hysteretic energy dissipation (Fig. 13) in pseudo-static tests, it also decreases the residual deformations (Fig. 14).

MODELING RECOMMENDATIONS

Figure 15 shows the generalized force-deformation relationship recommended in ASCE 41-17[25] and ACI 369.1-17[30] for diagonally reinforced coupling beams. The lines connecting points A through E represent the envelope response, where point B is the notional yield point, C the strength or peak force, D the post-peak strength, and E the point after which strength becomes negligible. Force-deformation values associated with these points are defined for diagonally reinforced coupling beams in Table 10-19 of ASCE 41-17 using parameters *c*, *d*, and *e*, as shown in Table 4 under the "Envelope A" heading. Table 4 also includes an alternative to ASCE 41-17 parameters recommended in TBI[31] (Envelope B). The deformations associated with

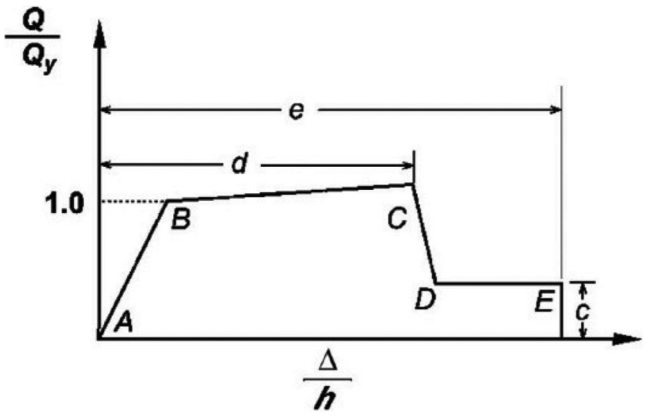

Fig. 15—Generalized force-deformation relationship defined in ASCE 41 Tables 10 through 19[25] and ACI 369.1 Table 19.[30]

parameters *d* and *e* in Table 4 refer to total deformation instead of plastic deformation.

Figure 16 shows the backbone curves (envelopes) for the four specimens described herein. The backbone curves represent line segments linking the points of peak shear attained during each step of the loading protocol (Fig. 5). Figure 16 also shows Envelopes A and B based on parameter values in Table 4. For calculation of the coordinates of point B, ASCE 41-17 and ACI 369.1-17 recommend the use of expected material properties, herein taken as f_{cm} and 1.1 times the specified f_y. Although ASCE 41-17 and ACI 369.1-17 recommend using an expected concrete compressive strength of $1.5f_c'$, this value was not appropriate for use on specimens tested within a few months of construction. For calculation of the force at Point C, a stress of 1.25 times the specified f_y was assumed in the diagonal reinforcement, which is the stress ACI 318[12] recommends for calculation of probable moment strength. The figures show the coupling beams attained larger strength and deformation than the envelopes defined by the parameter values in Table 4.

Figure 16 shows that for CB1 with Grade 60 (420) diagonal reinforcement, Envelope A overestimates the effective

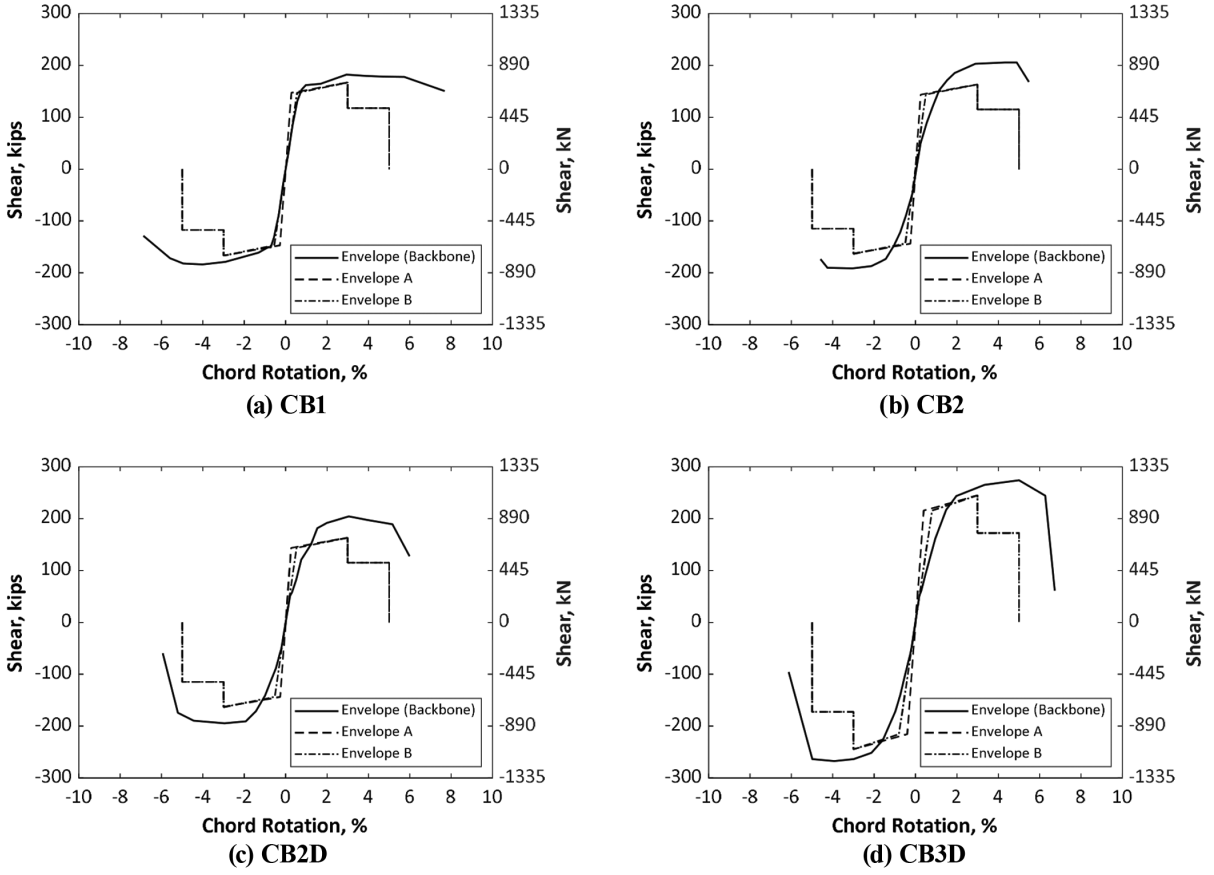

Fig. 16—Envelopes of shear versus chord rotation compared with other modeling parameters.

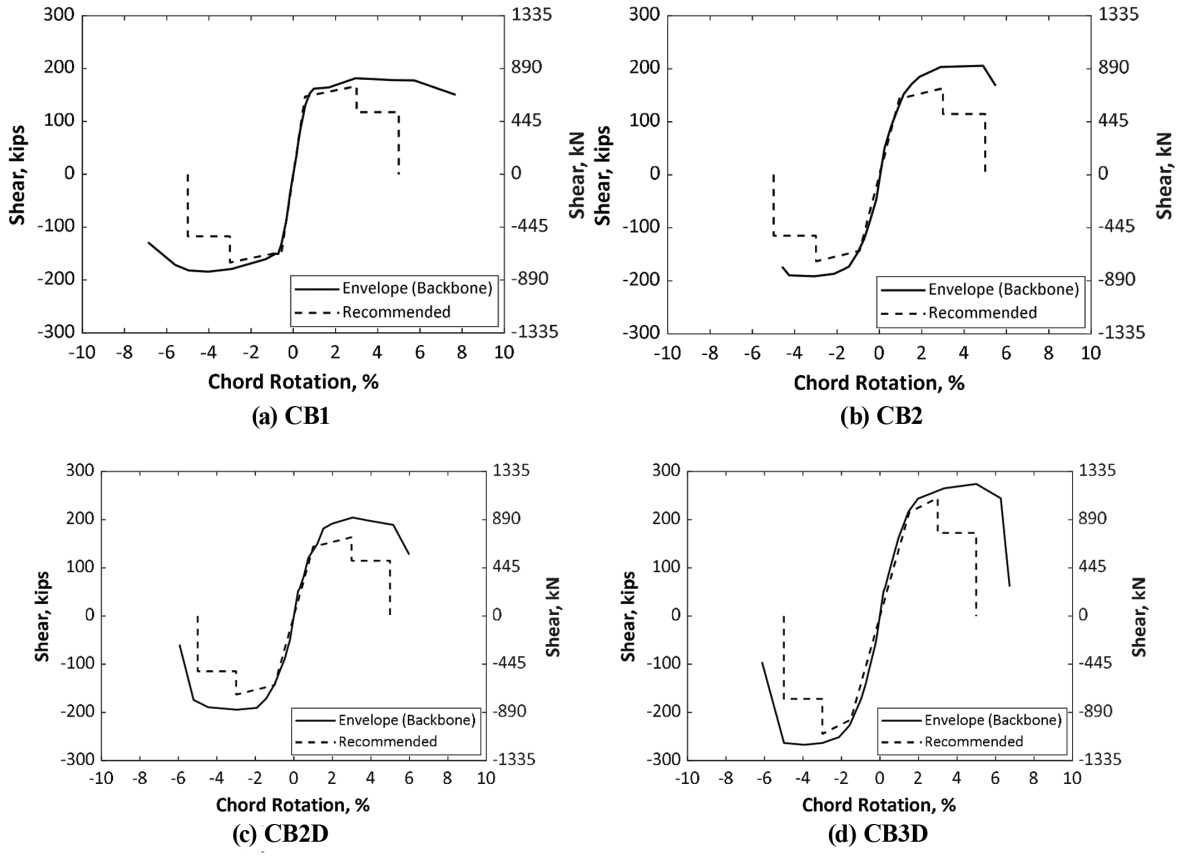

Fig. 17—Envelopes of shear versus chord rotation compared with proposed modeling parameters.

stiffness, but Envelope B closely matches it. Both Envelopes A and B overestimate the effective stiffness of the other specimens, which were constructed with smaller amounts of Grade 120 (830) diagonal reinforcement. To better represent the stiffness of coupling beams with different grades of diagonal reinforcement, it is recommended that stiffness be multiplied by $60/f_y$ in ksi ($420/f_y$ in MPa), as shown in the last column of Table 4.

Figure 17 shows the backbone curves from the measured envelopes for the four coupling beams of this study and the recommended envelope defined in Table 4. The figures indicate that the recommended envelope has an effective stiffness that closely matches the stiffness of all four coupling beams.

SUMMARY AND CONCLUSIONS

Results are reported from tests of four diagonally reinforced concrete coupling beams designed to study the behavior of coupling beams reinforced with high-strength Grade 120 (830) steel under pseudo-static reversed cyclic displacements. The main variables were yield stress of the diagonal reinforcement, nominal beam shear stress, and embedment length of the secondary (non-diagonal) longitudinal reinforcement. The following conclusions were drawn based on these tests and analyses:

1. Grade 120 (830) diagonal reinforcement may be an acceptable alternative to Grade 60 (420) diagonal reinforcement in terms of chord rotation capacity. Chord rotation capacities of specimens with Grade 60 and 120 (420 and 830) diagonal reinforcement were 7.1% and between 5.1 and 5.6%, respectively, which all exceed the expected chord rotation capacities from ASCE 41.[25]

2. Chord rotation capacities were limited by bar fracture after buckling in a prior cycle. Therefore, a likely cause of the difference in chord rotation capacities was the transverse reinforcement spacing, $3.4d_b$ and $4d_b$ for specimens with Grade 60 and 120 (420 and 830) bars, respectively, which made the Grade 120 (830) bars more prone to buckling.

3. A change from Grade 60 to 120 (420 to 830) bars resulted in an approximately 40% reduction in initial effective stiffness and 50% reduction in both hysteretic energy dissipation and residual chord rotation (for chord rotations between 3 and 5%). These properties were therefore approximately proportional to $60/f_y$ in ksi ($420/f_y$ in MPa). The extent to which these differences would affect the peak and residual drifts of a full-scale structure under dynamic excitation was outside the scope of this study. Further investigation is needed.

4. The 2017 Tall Building Initiative Report recommends $I_{eff} = 0.07(l_n/h)I_g$ for diagonally-reinforced coupling beams. When multiplied by $60/f_y$ in ksi ($420/f_y$ in MPa), this closely matched the stiffness of the coupling beams of this study.

5. Design for nominal shear stresses larger than $10\sqrt{f_c'}$, psi ($0.83\sqrt{f_c'}$, MPa) may be feasible in well detailed diagonally reinforced coupling beams. The coupling beam (CB3D) designed for a nominal shear stress of $14\sqrt{f_c'}$, psi ($1.17\sqrt{f_c'}$, MPa), 40% more than the ACI Building Code limit, exhibited a chord rotation capacity and mode of failure similar to the other coupling beams with high-strength Grade 120 (830) diagonal reinforcement. The shear strength of CB3D reached $19(\sqrt{f_{cm}})bh$ at a chord rotation of approximately 5% in both loading directions.

6. Coupling beams with non-diagonal longitudinal reinforcement cutoff near the wall face exhibited localized damage at the beam-wall interface; extending those bars into the end blocks caused damage to be more distributed throughout the beam span. This difference in detailing did not cause a change in deformation capacities, likely because diagonal bar buckling occurred at similar chord rotation demands regardless of the non-diagonal longitudinal reinforcement detail.

AUTHOR BIOS

Shahedreen Ameen *is a Project Consultant at Simpson Gumpertz & Heger Inc., New York, NY. She received her B.S. from Bangladesh University of Engineering and Technology, Dhaka, Bangladesh, in 2007, and her PhD from The University of Kansas, Lawrence, KS, in 2019.*

ACI member **Rémy D. Lequesne** *is an Associate Professor at The University of Kansas. He received his BSE, MSE, and PhD from the University of Michigan, Ann Arbor, MI. He is Chair of ACI Committee 408, Bond and Development of Steel Reinforcement, and member of ACI Committee 352, Joints and Connections in Monolithic Concrete Structures, and ACI Subcommittee 318-J, Joints and Connections (Structural Concrete Building Code).*

Andrés Lepage, *FACI, is a Professor at The University of Kansas. He received his PhD in civil engineering from the University of Illinois at Urbana-Champaign, Champaign, IL. He is a member of ACI Committees 318, Structural Concrete Building Code; 335, Composite and Hybrid Structures; 374, Performance-Based Seismic Design of Concrete Buildings; and 375, Performance-Based Design of Concrete Buildings for Wind Loads.*

ACKNOWLEDGMENTS

Primary financial support was provided by the Department of Civil, Environmental & Architectural Engineering and the School of Engineering at The University of Kansas. Partial support was provided by MMFX Technologies Corporation and Commercial Metals Company.

NOTATION

b_w	=	beam width, in. (mm)
CR	=	chord rotation
CR_{75}	=	chord rotation associated with V_{75}
CR_{cap}	=	chord rotation capacity obtained from the average of CR_{max}
CR_{max}	=	maximum chord rotation attained in a loading direction while maintaining 80% of maximum applied shear in that direction
c	=	parameter used for residual strength (Fig. 15)
D_m	=	peak displacement during a loading cycle, in. (mm)
d	=	parameter used for total deformation to capping point C (Fig. 15)
E_c	=	modulus of elasticity of concrete, ksi (MPa)
E_h	=	hysteretic energy dissipation index
e	=	parameter used for total deformation to point E (Fig. 15)
f_c'	=	specified concrete compressive strength, psi (MPa)
f_{cm}	=	average measured concrete compressive strength, psi (MPa)
f_y	=	specified yield stress of reinforcement, ksi (MPa)
f_{ym}	=	measured yield stress of reinforcement, ksi (MPa)
h	=	overall depth of beam, in. (mm)
I_{eff}	=	effective moment of inertia, in.^{4} (mm^4)
I_g	=	moment of inertia of gross concrete section about centroidal axis, neglecting reinforcement, in.^{4} (mm^4)
l_n	=	beam clear span measured from top of bottom block to bottom of top block, in. (mm)
Q_C	=	force at capping point C (Fig. 15)
Q_y	=	force at yielding point B (Fig. 15)
V_{75}	=	75% of the maximum shear in each loading direction, kip (kN)
V_m	=	force associated with peak displacement D_m, kip (kN)
V_{max}	=	maximum measured shear force, kip (kN)
V_n	=	nominal shear strength, kip (kN), based on expected material properties (Table 4)
V_{pr}	=	probable shear strength, kip (kN), based on $1.25f_y$ (Table 4)
v_{max}	=	shear stress calculated as $V_{max}/(b_w h)$, psi (MPa)

W = amount of hysteretic energy dissipated per cycle for each loading direction resisting force V_m at peak displacement D_m

ε_{su} = strain at peak stress, measured in accordance with ASTM E8[22]

REFERENCES

1. Paulay, T., and Binney, J. R., "Diagonally Reinforced Coupling Beams of Shear Walls," *Shear in Reinforced Concrete*, V. SP-42, 1974, American Concrete Institute, Farmington Hills, MI, pp. 579-598.

2. Naish, D.; Fry, A.; Klemencic, R.; and Wallace, J., "Reinforced Concrete Coupling Beams—Part 1: Testing," *ACI Structural Journal*, V. 110, No. 6, Nov.-Dec. 2013, pp. 1057-1066.

3. Shiu, K. N.; Barney, G. B.; Fiorato, A. E.; and Corley, W. G., "Reversing Load Tests of Reinforced Concrete Coupling Beams," Central American Conference on Earthquake Engineering – Conferencia Centroamericana de Ingeniería Sísmica, Proceedings, San Salvador, El Salvador, 1978, pp. 239-249.

4. Tegos, I. A., and Penelis, G. G., "Seismic Resistance of Short Columns and Coupling Beams Reinforced with Inclined Bars," *ACI Structural Journal*, V. 85, No. 1, Jan.-Feb. 1988, pp. 82-88.

5. Tassios, T. P.; Moretti, M.; and Bezas, A., "On the Behavior and Ductility of Reinforced Concrete Coupling Beams of Shear Walls," *ACI Structural Journal*, V. 93, No. 6, Nov.-Dec. 1996, pp. 711-720.

6. Galano, L., and Vignoli, A., "Seismic Behavior of Short Coupling Beams with Different Reinforcement Layouts," *ACI Structural Journal*, V. 97, No. 6, Nov.-Dec. 2000, pp. 876-885.

7. Lim, E.; Hwang, S.-J.; Wang, T.-W.; and Chang, Y.-H., "An Investigation on the Seismic Behavior of Deep Reinforced Concrete Coupling Beams," *ACI Structural Journal*, V. 113, No. 2, Mar.-Apr. 2016, pp. 217-226. doi: 10.14359/51687939

8. Choi, Y.; Hajyalikhani, P.; and Chao, S.-H., "Seismic Performance of Innovative Reinforced Concrete Coupling Beam—Double-Beam Coupling Beam," *ACI Structural Journal*, V. 115, No. 1, Jan. 2018, pp. 113-125. doi: 10.14359/51700951

9. Lequesne, R. D.; Parra-Montesinos, G. J.; and Wight, J. K., "Seismic Behavior and Detailing of High-Performance Fiber-Reinforced Concrete Coupling Beams and Coupled Wall Systems," *Journal of Structural Engineering*, ASCE, V. 139, No. 8, 2013, pp. 1362-1370. doi: 10.1061/(ASCE)ST.1943-541X.0000687

10. Parra-Montesinos, G. J.; Wight, J. K.; and Setkit, M., "Earthquake-Resistant Coupling Beams without Diagonal Reinforcement," *Concrete International*, V. 32, No. 12, Dec. 2010, pp. 36-40.

11. Harries, K. A.; Mitchell, D.; Cook, W. D.; and Redwood, R. G., "Seismic Response of Steel Beams Coupling Concrete Walls," *Journal of Structural Engineering*, ASCE, V. 119, No. 12, 1993, pp. 3611-3629. doi: 10.1061/(ASCE)0733-9445(1993)119:12(3611)

12. ACI Committee 318, "Building Code Requirements for Structural Concrete (ACI 318-14) and Commentary," American Concrete Institute, Farmington Hills, MI, 2014, 520 pp.

13. Cheng, M.-Y.; Gitomarsono, J.; and Zeng, H.-Y., "Cyclic Test of Diagonally Reinforced Concrete Coupling Beam with Different Shear Demand," *ACI Structural Journal*, V. 116, No. 6, Nov. 2019, pp. 241-250. doi: 10.14359/51718010

14. ATC 115, "Roadmap for the Use of High-Strength Reinforcement in Reinforced Concrete Design," Applied Technology Council, Redwood City, CA, 2014, 197 pp.

15. Lequesne, R. D.; Parra-Montesinos, G.; and Wight, J., "Seismic Response of Fiber-Reinforced Concrete Coupled Walls," *ACI Structural Journal*, V. 113, No. 3, May-June 2016, pp. 435-445. doi: 10.14359/51688822

16. ASTM C39/C39M-17a, "Standard Test Method for Compressive Strength of Cylindrical Concrete Specimens," ASTM International, West Conshohocken, PA, 2017, 8 pp.

17. ASTM A370-17, "Standard Test Methods and Definitions for Mechanical Testing of Steel Products," ASTM International, West Conshohocken, PA, 2017, 49 pp.

18. ASTM C33/C33M-16, "Standard Specification for Concrete Aggregates," ASTM International, West Conshohocken, PA, 2016, 11 pp.

19. ASTM C494/C494M-16, "Standard Specification for Chemical Admixtures for Concrete," ASTM International, West Conshohocken, PA, 2016, 10 pp.

20. ASTM A706/A706M-15, "Standard Specification for Deformed and Plain Low-Alloy Steel Bars for Concrete Reinforcement," ASTM International, West Conshohocken, PA, 2015, 7 pp.

21. ASTM A1035/A1035M-16a, "Standard Specification for Deformed and Plain, Low-Carbon, Chromium, Steel Bars for Concrete Reinforcement," ASTM International, West Conshohocken, PA, 2016, 8 pp.

22. ASTM E8/E8M-16a, "Standard Test Methods for Tension Testing of Metallic Materials," ASTM International, West Conshohocken, PA, 2016, 30 pp.

23. FEMA 461, "Interim Testing Protocols for Determining the Seismic Performance Characteristics of Structural and Nonstructural Components," Applied Technology Council, Redwood City, CA, 2007, 113 pp.

24. Ameen, S.; Lequesne, R. D.; and Lepage, A., "Diagonally-Reinforced Concrete Coupling Beams with High-Strength Steel Bars," SM Report No. 138, University of Kansas Center for Research, Inc., Lawrence, KS, 2020, 346 pp.

25. ASCE/SEI 41-17, "Seismic Evaluation and Retrofit of Existing Buildings," American Society of Civil Engineers, Reston, VA, 2017, 576 pp.

26. Huq, M. S.; Weber-Kamin, A. S.; Ameen, S.; Lequesne, R. D.; and Lepage, A., "High-Strength Steel Bars in Earthquake-Resistant T-Shaped Concrete Walls," SM Report No. 128, University of Kansas Center for Research, Inc., Lawrence, KS, 2018, 373 pp.

27. Park, R., "State-of-the-Art Report: Ductility Evaluation from Laboratory and Analytical Testing," *Ninth World Conference on Earthquake Engineering*, Proceedings, Tokyo-Kyoto, Japan, 1988, pp. 605-616.

28. Elwood, K. J., and Eberhard, M. O., "Effective Stiffness of Reinforced Concrete Columns," *ACI Structural Journal*, V. 106, No. 4, July-Aug. 2009, pp. 476-484.

29. Otani, S., "Hysteresis Models of Reinforced Concrete for Earthquake Response Analysis," *The University of Tokyo Journal of the Faculty of Engineering*, V. 36, No. 2, 1981, pp. 125-159.

30. ACI Committee 369, "Standard Requirements for Seismic Evaluation and Retrofit of Existing Concrete Buildings (ACI 369.1-17) and Commentary," American Concrete Institute, Farmington Hills, MI, 2017, 110 pp.

31. PEER TBI, *Guidelines for Performance-Based Seismic Design of Tall Buildings*. Pacific Earthquake Engineering Research Center, Tall Buildings Initiative, Report No. 2017/06, University of California, Berkeley, CA, 2017, 143 pp.